Lineage-specific laminar organization of cortical GABAergic interneurons

Gabriele Ciceri[1], Nathalie Dehorter[1], Ignasi Sols[1], Z Josh Huang[2], Miguel Maravall[1] & Oscar Marín[1]

In the cerebral cortex, pyramidal cells and interneurons are generated in distant germinal zones, and so the mechanisms that control their precise assembly into specific microcircuits remain an enigma. Here we report that cortical interneurons labeled at the clonal level do not distribute randomly but rather have a strong tendency to cluster in the mouse neocortex. This behavior is common to different classes of interneurons, independently of their origin. Interneuron clusters are typically contained within one or two adjacent cortical layers, are largely formed by isochronically generated neurons and populate specific layers, as revealed by unbiased hierarchical clustering methods. Our results suggest that different progenitor cells give rise to interneurons populating infra- and supragranular cortical layers, which challenges current views of cortical neurogenesis. Thus, specific lineages of cortical interneurons seem to be produced to primarily mirror the laminar structure of the cerebral cortex, rather than its columnar organization.

Brain circuitries have evolved as complex networks of excitatory and inhibitory neurons. In the cerebral cortex, excitatory glutamatergic pyramidal cells and inhibitory GABAergic interneurons constitute the main cellular elements of the individual circuits. Pyramidal cells specialize in transmitting information between different cortical regions and to other regions of the brain. Interneurons comprise a heterogeneous group of neurons that shape various forms of collective activity and that primarily contribute to local assemblies, where they provide inhibitory inputs that modulate the responses of pyramidal neurons[1,2].

Pyramidal cells and interneurons are organized along two main axes in the cortex. A first axis divides the cortex into a variable number of layers, depending on cortical area. Neurons within the same cortical layer share important features, including general patterns of connectivity[3]. The second axis reflects the vertical organization of neuronal circuits within a column of cortical tissue. Neurons within a given column are stereotypically interconnected in the vertical dimension, share extrinsic connectivity and function as basic units underlying cortical operations[4,5]. Thus, any cortical area consists of a sequence of columns in which the main cellular constituents, pyramidal cells and interneurons, share a common organization[6]. Understanding the mechanisms that control the distribution of excitatory and inhibitory neurons in each of these repetitive elements is essential to comprehending the fundamental organization of the cortex.

One challenge for elucidating the mechanisms underlying the formation of neural assemblies in the cortex is that pyramidal cells and interneurons are born in separate and distant germinal zones. Thus, while pyramidal cells are produced in the ventricular zone of the pallium and migrate radially to reach their final position[7,8], interneurons are generated in the subpallium and migrate to the cortex via a long tangential migration before acquiring their definitive laminar position[9,10]. The challenge is further complicated by the large diversity of cortical interneurons, which are generated from various progenitor pools[11–15], migrate through partially different routes[16–18] and adopt their final laminar position following distinct rules[19,20].

Cortical interneurons originate from three main sources in the developing subpallium: (i) the medial ganglionic eminence (MGE), which gives rise to fast-spiking (FS), parvalbumin-expressing (PV[+]) interneurons and to non-fast-spiking (NFS), somatostatin-expressing (SST[+]) interneurons; (ii) the caudal ganglionic eminence (CGE), which is the source of rapidly adapting, typically bipolar interneurons that express calretinin and/or vasointestinal peptide (VIP^{+} neurons) and of multipolar interneurons that contain neuropeptide Y and/or reelin but not SST; and (iii) the preoptic area (POA), which produces a small but very heterogeneous fraction of cortical interneurons[15,21]. All main classes of interneurons are found throughout the cortex, but their respective laminar allocation varies. For example, while PV[+] and SST[+] interneurons colonize more or less evenly the entire thickness of the cortex, VIP[+] interneurons are primarily found in superficial layers[19,22–24]. The laminar distribution of cortical interneurons correlates with the birthdate of MGE-derived cells but not that of CGE-derived interneurons[19,23,25,26]. Thus, it is unlikely that the same mechanisms could govern the integration of different classes of GABAergic interneurons into each of the repetitive columnar microcircuits of the cortex.

It has been suggested that interneurons may distribute throughout the cortex following random patterns of migration[27,28]. In contrast, recent work indicated that interneurons derived from the MGE or POA (MGE/POA-derived) do not distribute randomly but rather form spatially organized clusters[29]. It is unclear, however, whether this is a general behavior for all main classes of cortical interneurons and, if so, whether they adopt a predictable pattern of organization in relation to the laminar or columnar organization of the cortex.

---

[1]Instituto de Neurociencias, Consejo Superior de Investigaciones Científicas & Universidad Miguel Hernández, Sant Joan d'Alacant, Spain. [2]Cold Spring Harbor Laboratory, Cold Spring Harbor, New York, USA. Correspondence should be addressed to M.M. (mmaravall@umh.es) or O.M. (o.marin@umh.es).

RESULTS

Region-specific labeling of progenitor cells in the subpallium

To study the organization of interneurons in the cortex, we explored the distribution of small cohorts of interneurons derived from a limited number of progenitor cells. Replication-incompetent retroviral vectors encoding reporter genes have been widely used for the analysis of lineage relationships during brain development[30]. These viral vectors can infect mitotic cells only, and so this approach allows the identification of the progeny of cells. One limitation of this method, however, is that it marks progenitor cells indiscriminately, which limits its potential in clonal analyses. To circumvent this limitation, we combined retroviral labeling with the Cre-loxP system, a genetic method that allows the irreversible labeling of cells with a specified gene expression history. In brief, we generated a conditional expression system consisting of an enhanced green fluorescent protein gene (*Gfp*) that is silent in the absence of Cre activity but that leads to the expression of the reporter protein after Cre-mediated recombination (**Supplementary Fig. 1a**). Retroviral vectors based on this system (rv::dio-Gfp) likewise infect progenitor cells indiscriminately, but only those expressing Cre recombinase and their progeny will ultimately express *Gfp*. Consistently, the brain of wild-type mice infected with retroviral particles encoding the conditional cassette did not contain GFP-expressing (GFP+) cells (**Supplementary Fig. 1b–d**), while infection of mouse embryos with ubiquitous Cre expression throughout the ventricular zone led to widespread labeling of GFP+ clones (**Supplementary Fig. 1e–g**).

We used this method to specifically label progenitor cells in the MGE/POA region using mouse embryos expressing Cre recombinase under the control of the promoter sequence of *Nkx2-1*, which encodes a transcription factor expressed by progenitor cells in these regions[31] (**Fig. 1a**). Delivery of a high-titer retroviral stock into the lateral ventricle of *Nkx2-1-Cre* embryos at embryonic day (E) 11.5 using ultrasound-guided imaging led to robust but highly specific labeling of MGE/POA progenitor cells throughout the rostrocaudal extent of the telencephalon (**Fig. 1b,c**). Immunohistochemical analysis confirmed that labeled cells were confined to Nkx2-1+ territories, even though no limitations exist for viral infection (*n* = 10, **Fig. 1b–e**). This method therefore allows the specific labeling of progenitor cells with high fidelity.

Tagging interneuron progenitor cells at clonal density

We then carried out experiments at progressively more diluted concentrations to achieve labeling of MGE/POA progenitor cells at clonal density (**Fig. 1f**). When low-titer injections at E11.5 were examined 2 d later, we observed a limited number of clusters containing GFP+ cells in the MGE and POA (**Fig. 1g**). These clusters were randomly scattered throughout these territories, with no particular spatial bias. They typically contained a single cell with radial glia–like morphology and a variable number of other cells with no apparent contact with the ventricle (**Fig. 1h**). In addition, we also observed some GFP+ cells that were not close to a cell with radial glia-like morphology. Because retroviruses integrate randomly into one of the daughter cells of the infected progenitor, we reasoned that these isolated cells were likely the result of an integration event in a postmitotic neuron or an intermediate progenitor cell (IPC) (**Fig. 1a**).

The observation of isolated clusters suggested that they contained clonally related cells. To confirm this, we infected E11.5 *Nkx2-1-Cre* mouse embryos with a low-titer mixture of two conditional reporter retroviral vectors, encoding GFP or the red fluorescent protein
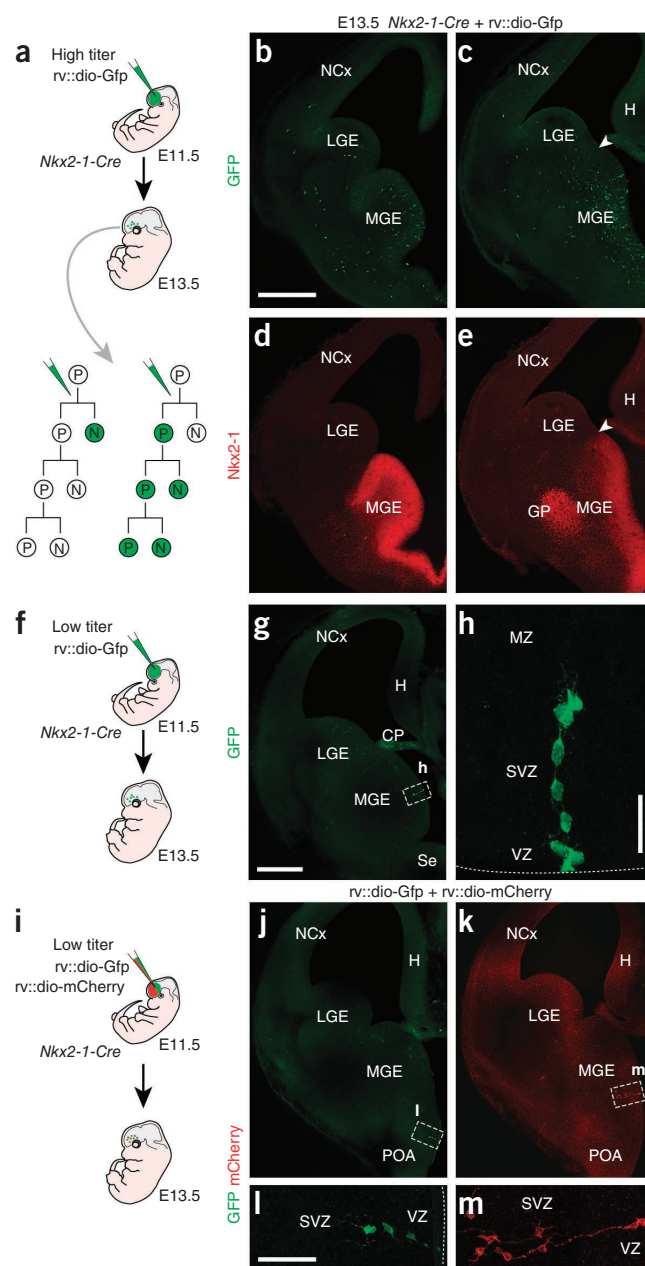
Figure 1 Region-specific labeling of progenitor cells with conditional retroviruses. (**a**) The experimental model for **b**–**e**. Retroviruses randomly integrate into one of the daughter cells, which may lead to the incomplete or complete labeling of the clone. P, progenitor cell; N, neuron. (**b**–**e**) Coronal sections through the telencephalon of an E13.5 *Nkx2-1-Cre* embryo infected with high-titer conditional reporter retroviruses at E11.5 and stained with antibodies against GFP (**b,c**) and Nkx2-1 (**d,e**). (**f**) The experimental model for **g,h**. (**g,h**) Coronal section through the telencephalon of an E13.5 *Nkx2-1-Cre* embryo infected with low-titer conditional reporter retroviruses at E11.5 and stained with antibodies against GFP. Panel **h** is a high-magnification image of an individual clone of GFP-labeled cells. (**i**) The experimental model for **j**–**m**. (**j**–**m**) Coronal sections through the telencephalon of an E13.5 *Nkx2-1-Cre* embryo infected with GFP and mCherry low-titer conditional reporter retroviruses at E11.5 and stained with antibodies against GFP and mCherry. Panels **l** and **m** are high magnification images of the boxed areas in **j** and **k**, respectively. CP, choroid plexus; GP, globus pallidus; H, hem; LGE, lateral ganglionic eminence; MGE, medial ganglionic eminence; NCx, neocortex; POA, preoptic area; Se, septum; Str, striatum; VZ, ventricular zone; SVZ, subventricular zone. Dashed lines define the ventricular surface. Scale bars, 300 μm (**b**–**e**), 250 μm (**g,j,k**), 50 μm (**h**), 100 μm (**l,m**).

mCherry (**Fig. 1i**). Analysis of these experiments at E13.5 revealed that GFP$^+$ and mCherry$^+$ cells typically segregated into distinct clusters (**Fig. 1j–m**).
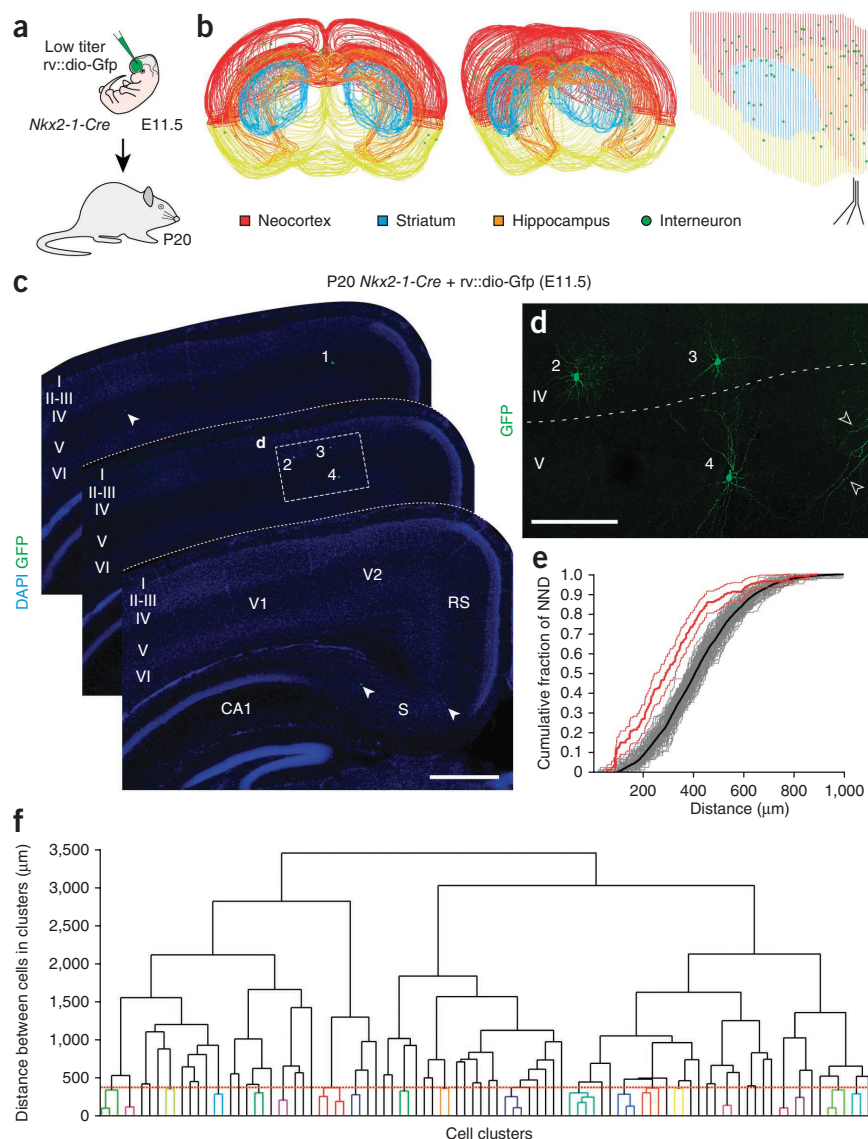
MGE/POA-derived interneurons cluster in the cortex

We used this method to examine whether distinct classes of interneurons use different strategies to achieve their final distribution in the cerebral cortex. We performed low-titer injections of conditional reporter retroviral stocks in the lateral ventricle of E11.5 *Nkx2-1-Cre* embryos and examined the distribution of labeled interneurons in the neocortex of postnatal day (P) 20 mice, a stage at which interneurons have adopted their final position in the cortex (**Fig. 2a**). These long-term experiments yielded a relatively small number of labeled cells (ranging from ~30 to ~300 cells, depending on the experiment) in the entire neocortex of infected mice. We examined more than 100 cells from three different mice and confirmed that the GFP$^+$ or mCherry$^+$ cells had morphological features of interneurons and were immunoreactive for GABA (data not shown).

We plotted the position of each population of labeled cells in the neocortex using serial section reconstructions and analyzed their distribution and spatial relationships (**Fig. 2b**). Labeled interneurons were always distributed throughout the rostrocaudal extent of the cortex, with no particular spatial bias. However, we observed that many interneurons appeared in discrete clusters of cells that were spatially segregated from one another (**Fig. 2c,d**). To determine whether labeled interneurons were randomly distributed, we calculated the distance from each interneuron to its closest neighbor (nearest neighbor distance, or NND) and constructed the resulting distribution of NNDs for each experimental population. For each data set, we then built NND distributions for 100 computer-simulated populations of randomly distributed neurons, generated using the same number of neurons in the same region of tissue as the real population. Comparison of NND distributions revealed strong differences in the spatial organization of experimental and simulated data sets (**Fig. 2e**; 93% of the comparisons between experimental and simulated data sets had a $P < 0.01$, Kolmogorov-Smirnov test, $n = 14$). Neurons in the experimental data sets were separated by shorter NNDs than neurons in the simulated, randomly distributed data sets (**Fig. 2e**). Thus, interneurons arising from a limited number of progenitor cells in the MGE/POA region do not distribute randomly throughout the neocortex.

Our empirical observations revealed that many interneurons grouped in clusters that spanned roughly 3×10^7 μm^3 of cortical volume. However, we also observed isolated interneurons throughout the cortex, which might correspond to the incomplete labeling of progenitor clones (**Fig. 1a**). To investigate the spatial distribution of interneuron clusters, we developed an unbiased and unsupervised

Figure 2 Clustering of MGE/POA-derived interneurons in the cerebral cortex. (**a**) The experimental model. (**b**) Three-dimensional reconstruction of the distribution of cortical interneurons in a P20 *Nkx2-1-Cre* mouse infected with low-titer conditional reporter retroviruses at E11.5. (**c,d**) Serial coronal sections (100 μm thick) through the telencephalon of a P20 *Nkx2-1-Cre* mouse infected with low-titer conditional reporter retroviruses at E11.5 and stained with DAPI and antibodies against GFP. Four labeled interneurons (labeled 1 to 4) form a small and compact cluster that spans two adjacent sections. Neurons 2 to 4 are shown at high magnification in **d**. Solid arrowheads in **c** point to other interneurons; open arrowheads in **d** indicate the dendrites of interneuron 1. Dashed lines define external brain boundaries in **c** and cortical layers in **d**. (**e**) Cumulative NNDs for an example population taken from one *Nkx2-1-Cre* mouse, with experimental (heavy red line) and simulated (black line) distributions. Light red lines delineate a $P = 0.05$ confidence interval for the experimental distribution; gray lines depict 100 random repetitions for the simulated distribution. Kolmogorov-Smirnov two-sample test, $P = 5.06 \times 10^{-25}$. (**f**) Dendrogram showing hierarchical relationships between labeled interneurons grouped according to their distances. The red dotted line indicates the threshold value that defines clustering for this experiment. I–VI, cortical layers I to VI; CA1, hippocampal CA1 area; RS, retrosplenial cortex; S, subiculum, V1, primary visual cortex; V2, secondary visual cortex. Scale bars, 300 μm (**c**), 100 μm (**d**).

1201

approach to group labeled cells into individual clusters on the basis of agglomerative hierarchical clustering methods. In brief, for each experimental condition, interneurons were grouped according to proximity relationships (average distance between neurons) and the result displayed in a dendrogram (**Fig. 2f**). The number of clusters in the experiment was then calculated using a threshold distance value that maximized the difference between the number of clusters observed in the experimental data set and the mean number of clusters in 100 simulated populations of randomly distributed neurons, using the same number of neurons in the same region. One advantage of the algorithm is that it is dimensionality-unbiased; that is, no particular dimension bias is introduced in the identification of interneuron clusters, and only the distance between cells factors into their grouping. Using this method, we found that a large fraction of labeled interneurons clustered in the cortex in all experimental data sets (68.23 ± 3.56% of interneurons in clusters, mean ± s.e.m., $n = 10$). These experiments yielded ~50 clusters per data set (49.92 ± 10.29, $n = 12$). The average distance between interneurons in a cluster was remarkably consistent across different brains (mean threshold distance value 389 ± 18 μm, $n = 10$), which suggested that our analysis consistently identified cell clusters in an unsupervised manner.
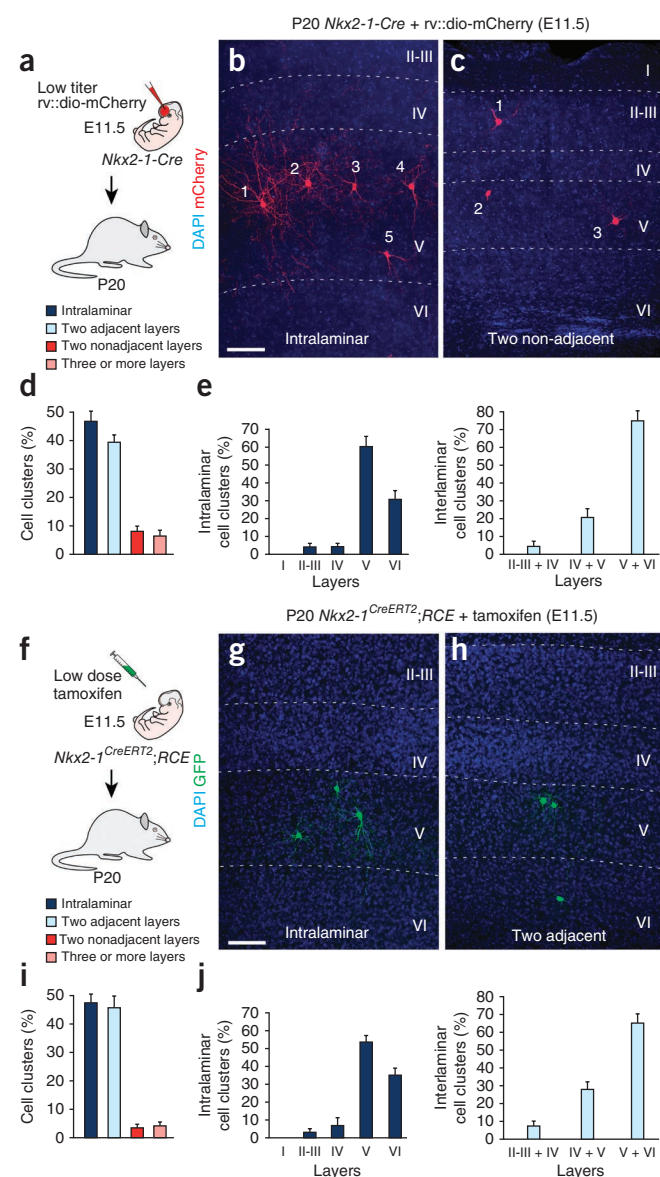
Interneuron clustering might be linked to lineage relationships or arise as a non–cell-autonomous property of cortical interneurons. Although our short-term analyses suggested that low-titer retroviral infections typically labeled individual clones (**Fig. 1j–m**), ultracentrifugation of retroviral stocks may produce viral clumps resulting in focal infections that resemble clones, even at limiting dilutions. To directly test this, we analyzed the distribution of labeled interneurons in the cortex of P20 *Nkx2.1-Cre* mice that were simultaneously infected with low-titer stocks of conditional retroviruses encoding green (GFP) and red (mCherry) reporters, mixed before ultracentrifugation[32]. As before, we used agglomerative hierarchical clustering to identify interneuron groups labeled with each of the reporter proteins independently. We next used the smaller threshold distance value obtained for these populations to identify interneuron clusters independently of the reporter protein, as if GFP+ and mCherry+ interneurons were derived from the same progenitor cells. Under these conditions, we quantified the fraction of interneuron clusters that contained GFP+ and mCherry+ interneurons. We found that approximately 60% of clusters contained at least one interneuron labeled with a different fluorescent protein than the dominant one for that particular cluster (66.83 ± 1.40% mixed clusters, $n = 6$; **Supplementary Fig. 2**). Thus,

although clusters contained clonally related interneurons, most clusters were likely to include cells from a different progenitor, even at very limiting dilutions. This strongly suggested that lineage relationships are not exclusive determinants of interneuron clustering.

Spatial organization of MGE/POA-derived interneuron clusters

We used the dendrograms derived from the agglomerative hierarchical clustering analysis to examine the spatial organization of individual interneurons within clusters. We found that most cell clusters contained interneurons located within a single layer of the cortex or in two adjacent layers (intralaminar, 46.85 ± 4.06%; adjacent interlaminar, 39.45 ± 2.14%; $n = 10$; **Fig. 3a–d**). In contrast, the percentage of clusters with cells that spanned two nonadjacent layers or three or more layers was very small (nonadjacent, 8.22 ± 2.20%; three or more, 6.60 ± 2.33%; $n = 10$; **Fig. 3a–d**).

We next analyzed the laminar distribution of interneuron clusters. We found that intralaminar clusters labeled with retroviral infections at E11.5 did not distribute evenly throughout the cortex but rather concentrated in deep layers (clusters in layer V or VI, 91.18 ± 2.97%; $n = 10$; **Fig. 3e**). Even those clusters that spanned two adjacent layers resided

Figure 3 Spatial organization of MGE/POA-derived interneuron clusters. (**a**) The experimental model for **b**–**e**. (**b**,**c**) Coronal sections through the motor (**a**) and visual (**b**) cortices of a P20 *Nkx2.1-Cre* mouse infected with low-titer conditional reporter retroviruses at E11.5 and stained with the nuclear indicator DAPI and antibodies against mCherry. The images show examples of intralaminar (**b**) and interlaminar (**c**) interneuron clusters (cells labeled 1 to 5 and 1 to 3, respectively). (**d**) Quantification of the relative abundance of intralaminar and interlaminar (two adjacent, two nonadjacent, and three or more layers) interneuron clusters. (**e**) Quantification of the laminar distribution of intralaminar and interlaminar (two adjacent layers only) interneuron clusters. (**f**) The experimental model for **g**–**i**. (**g**,**h**) Coronal sections through the neocortex of a P20 *Nkx2.1CreERT2;RCE* mouse induced with a low tamoxifen dose at E11.5 and stained with DAPI and antibodies against GFP. The images show examples of intralaminar (**g**) and interlaminar (**h**) interneuron clusters. (**i**) Quantification of the relative abundance of intralaminar and interlaminar (two adjacent, two nonadjacent, and three or more layers) interneuron clusters. (**j**) Quantification of the laminar distribution of intralaminar and interlaminar (two adjacent layers only) interneuron clusters. I–VI, cortical layers I to VI. Dashed lines define cortical layers. Scale bars, 100 μm. Histograms depict mean ± s.e.m.

preferentially in the deep layers of the cortex (layer V or VI clusters, 74.97 ± 5.21%; $n = 10$; **Fig. 3e**). These results suggested that progenitor cells infected at E11.5 do not produce many interneurons that populate the superficial layers of the cerebral cortex. Instead, most of the lineages labeled in the MGE/POA at E11.5 seem to give rise almost exclusively to interneurons that occupy the infragranular layers of the cortex.

It is at least theoretically conceivable that we failed to observe interneurons in the superficial layers of the neocortex owing to viral silencing. To rule out this possibility, we used a different method to label interneuron lineages at clonal density. In brief, we crossed mice expressing a tamoxifen-inducible form of Cre (CreERT2) under the control of the *Nkx2-1* promoter region (*Nkx2-1^CreERT2* mice) with a general reporter allele (*RCE*, Rosa26 reporter CAG-boosted EGFP) and titrated the amount of tamoxifen required to elicit Cre recombination in MGE/POA progenitors at clonal density (**Supplementary Fig. 3a–d**). Subsequently, we induced Cre expression in E11.5 embryos and analyzed the distribution of labeled interneurons at P20 (**Fig. 3f**).

Analysis of the neocortex of P20 *Nkx2-1^CreERT2;RCE* mice exposed to low tamoxifen doses at E11.5 again revealed interneuron clustering in the neocortex (**Supplementary Fig. 3e,f**). NND comparisons between experimental and simulated data sets confirmed that the distribution of clonally related MGE/POA-derived interneurons was not random (100% of the comparisons between experimental and simulated data sets had a $P < 0.01$, Kolmogorov-Smirnov, $n = 8$; **Supplementary Fig. 3g**). Agglomerative hierarchical clustering methods revealed that the organization of individual clusters in *Nkx2-1^CreERT2;RCE* mice induced with low tamoxifen doses was very similar than in *Nkx2-1-Cre* mice infected with retroviruses (78.06 ± 3.16% of interneurons in clusters; 37.38 ± 7.54 clusters per data set, $n = 8$; mean threshold value 485 ± 39 μm; $n = 8$; **Supplementary Fig. 3h**). Most notably, interneuron clusters in *Nkx2-1^CreERT2;RCE* mice were largely restricted to one or two adjacent layers of the cortex (intralaminar, 47.49 ± 4.33%; adjacent interlaminar, 45.28 ± 4.37; $n = 8$; **Fig. 3g–i**) and were typically confined to deep layers of the neocortex (clusters in layer V or VI, 89.39 ± 3.98; $n = 8$; **Fig. 3j**). These experiments confirmed that the MGE/POA at E11.5 primarily contains progenitor cells that generate interneurons for the infragranular layers of the cortex.

Most interneuron clusters contain coetaneous neurons

There is a strong correlation between time of birth and final laminar distribution in MGE-derived interneurons[25,26,33,34]. To test this idea at clonal levels, we analyzed the spatial organization of the clusters in relation to the timing of neurogenesis of their constituent interneurons. Specifically, we carried out birth-dating analyses at two different embryonic stages (E12.5 and E15.5) in retroviral lineage tracing experiments ($n = 43$ clusters from three different experiments; **Supplementary Fig. 4a**). In these experiments, we defined isochronic clusters as those containing a majority of cells born in the same stage and no cells born in the alternative age, and heterochronic clusters as those containing at least one cell born at E12.5 and another one at E15.5. We found that all intralaminar clusters were isochronic ($n = 28$ of 28 clusters; **Supplementary Fig. 4b,d**), whereas all clusters that spanned several layers were heterochronic ($n = 4$ of 4 clusters; **Supplementary Fig. 4c,d**). The organization of clusters spanning two adjacent layers was more diverse, with roughly half of the clones classified as isochronic ($n = 6$ of 11 clusters) and the other half heterochronic ($n = 5$ of 11 clusters; **Supplementary Fig. 4d**).

The finding of multiple neurons with highly correlated birthdates in most intralaminar clusters suggested that these clones might be generated through the expansion of cell lineages by way of intermediate progenitor cells (IPCs), which would become neurogenic at roughly the same time. To test this hypothesis, we first examined the expression of
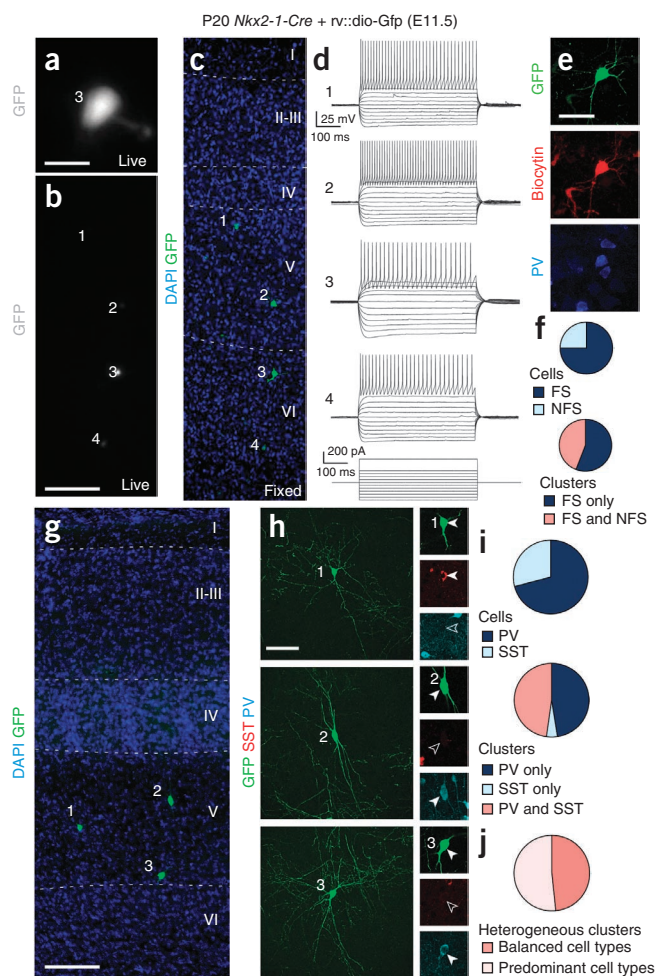
Figure 4 Electrophysiological and neurochemical characterization of MGE/POA-derived interneuron clusters. (**a,b**) Live imaging of a coronal section through the somatosensory cortex of a P20 *Nkx2-1-Cre* mouse infected with low-titer conditional reporter retroviruses at E11.5 showing a cluster of four GFP+ interneurons (labeled 1 to 4). The high-magnification image (**a**) was acquired during patch-clamp recording. (**c**) The same coronal section shown in **b** stained with DAPI and antibodies against GFP. (**d**) Current-clamp recordings in whole-cell configuration reflecting the response of interneurons (labeled 1 to 4) in the cluster to current steps. Cells were recorded using a pipette containing biocytin. (**e**) Expression of GFP and PV and biocytin fluorescence in one of the interneurons in the cluster shown in **b** and **c**. (**f**) Quantification of the percentage of FS and NFS cells in interneuron clusters, as well as the fraction of clusters that contained only FS cells or both FS and NFS cells. (**g,h**) Coronal section through the somatosensory cortex of a P20 *Nkx2-1-Cre* mouse infected with low-titer conditional reporter retroviruses at E11.5 and stained with DAPI and antibodies against GFP, showing an intralaminar cluster (cells labeled 1 to 3). High-magnification images (**h**) show the morphology of these interneurons, two of which (cells 2 and 3) express PV and the other of which (cell 1) expresses SST. (**i**) Quantification of the percentage of PV+ and SST+ cells in interneuron clusters, as well as the fraction of clusters that contained only PV+ cells, only SST+ cells or both PV+ and SST+ cells. (**j**) Quantification of the fraction of heterogeneous clusters that contained a predominant cell type or similar proportions of PV+ and SST+ cells. I–VI, cortical layers I to VI. Dashed lines define cortical layers. Scale bars, 20 μm (**a,e**), 50 μm (**h**), 100 μm (**b,c,g**; **b** and **c** have the same magnification).

the proliferation marker Ki67 in individual clones 40 h after retroviral infection (**Supplementary Fig. 5a**). We found that many GFP$^+$ cells in each individual clone expressed Ki67 at this stage (**Supplementary Fig. 5b–e**). This observation suggested that most interneuron clusters are formed through the expansion of individual lineages by way of IPCs. To confirm this idea, we infected E11.5 mouse embryos with retroviruses simultaneously encoding mCherry and a fluorescent, ubiquitylation-based cell cycle indicator (Fucci) that accumulates in the nucleus during S, G2 and M phases (**Supplementary Fig. 5f**). Consistent with the Ki67 results, we observed that interneuron clones contained a high percentage of IPCs 40 h after retroviral infection (**Supplementary Fig. 5g–l**). Taken together, these results suggest that most interneuron clones expand through IPCs that divide concurrently, which might explain the abundance of coetaneous interneurons in the clusters (**Supplementary Fig. 4**).

Characterization of MGE/POA-derived interneuron clusters

We wondered whether cortical clusters contain interneurons with similar electrophysiological and neurochemical properties. To address this question, we identified interneuron clusters in acute 300-μm serial sections through the cerebral cortex of P20–P30 *Nkx2-1-Cre* mice that were infected at E11.5, and recorded the intrinsic electrophysiological properties of interneurons in each of these clusters (**Fig. 4a–c**). Consistent with previous results[11], recorded cells exhibited one of the two main profiles found in MGE/POA-derived interneurons, FS and NFS firing in response

to a suprathreshold current injection. We found that a large proportion of clusters exclusively contained FS interneurons ($n = 5$ of 9 clusters; **Fig. 4d–f** and **Supplementary Fig. 6**). As expected, correlative immunohistochemical analysis revealed that these interneurons contained PV (**Fig. 4e,f**). We also found that many of the recorded clusters contained both FS and NFS interneurons ($n = 4$ out of 9 clusters; **Fig. 4f** and **Supplementary Fig. 6**). NFS interneurons typically contained the neuropeptide SST and were electrophysiologically heterogeneous (**Supplementary Fig. 6**).

We next analyzed the expression of PV and SST in a large cohort of clusters identified through agglomerative hierarchical clustering analysis ($n = 143$ clusters from two different experiments). Irrespective of their organization in clusters, we found that interneurons expressing PV outnumbered those expressing SST by a 3:1 proportion (70.99 ± 14.04% and 29.01 ± 7.52%, respectively; **Fig. 4g–i**), a finding that matches the normal proportion of cortical PV$^+$ and SST$^+$ interneurons[35]. Analysis of the neurochemical profile of interneurons within individual clusters revealed that approximately half of the clusters exclusively contained PV$^+$ interneurons ($n = 68$ out of 143 clusters, **Fig. 4i**), while only a very small fraction were uniformly made of SST$^+$ interneurons ($n = 7$ out of 143 clusters, **Fig. 4i**). The remaining clusters contained both PV$^+$ and SST$^+$ interneurons ($n = 68$ out of 143 clusters; **Fig. 4g–i**). Approximately half of the heterogeneous clusters contained a predominant interneuron class ($n = 32$ out of 68

Figure 5 Clustering of PV$^+$ interneurons in the cerebral cortex. (**a,b**) Serial coronal sections (100 μm thick) through the telencephalon of a P20 *Pvalb^{Cre}* mouse infected with low-titer conditional reporter retroviruses at E11.5 and stained with DAPI and antibodies against mCherry. Six labeled interneurons (1 to 6) form a large cluster that spans three adjacent sections. Neurons 3 to 5 are shown at high magnification in **b**. Solid arrowheads in **a** point to other labeled interneurons. Dashed lines define external brain boundaries in **a** and cortical layers in **b**. (**c**) Cumulative NNDs for an example population taken from one *Pvalb^{Cre}* mouse, with experimental (heavy red line) and simulated (black line) distributions. Light red lines delineate a $P = 0.05$ confidence interval for the experimental distribution; gray lines depict 100 random repetitions for the simulated distribution. Kolmogorov-Smirnov two-sample test, $P = 6.14 \times 10^{-21}$. (**d**) Dendrogram showing the hierarchical relationship between labeled PV$^+$ interneurons grouped according to their distances using agglomerative hierarchical clustering. The red dotted line indicates the threshold value that defines clustering for this experiment. (**e**) Quantification of the relative abundance of intralaminar and interlaminar (two adjacent, two nonadjacent, and three or more layers) interneuron clusters. (**f**) Quantification of the laminar distribution of intralaminar and interlaminar (two adjacent layers only) interneuron clusters. I–VI, cortical layers I to VI; Cg, cingulate cortex; CPu, caudoputamen nucleus; M1, primary motor cortex; M2, secondary motor cortex; S1, primary somatosensory cortex. Scale bars, 300 μm (**a**), 100 μm (**b**). Histograms depict mean ± s.e.m.

clusters; **Fig. 4j**), while the rest contained similar proportions of both interneuron classes (*n* = 36 out of 68 clusters; **Fig. 4j**).

## Reverse lineage tracing of MGE/POA interneurons

One advantage of the method that we developed for lineage analysis is that the combination of retroviral tracing and Cre-*lox*P technology can be extended using Cre lines that are unique to certain classes of interneurons, such as *Pvalb*^{Cre} and *Sst*^{Cre}. In these experiments, progenitor cells are indistinctly infected throughout the telencephalon, but only those that give rise to neurons expressing PV (*Pvalb*^{Cre} infections) or SST (*Sst*^{Cre} infections) will ultimately express the corresponding reporter fluorescent protein (GFP or mCherry). Because Cre expression is postmitotic in both *Pvalb*^{Cre} and *Sst*^{Cre} mice, clones cannot be monitored at embryonic stages, but their ability to cluster in the cortex can be assessed in P20 mice.

We first examined whether PV$^+$ interneurons cluster in the cerebral cortex, as predicted by our experiments in *Nkx2-1-Cre* mice. Analysis of the neocortex of P20 *Pvalb*^{Cre} mice infected with conditional retroviruses at E11.5 revealed that many labeled interneurons were indeed grouped in small clusters throughout the neocortex (**Fig. 5a,b**). Consistently, NND comparisons between experimental and simulated data sets confirmed that the distribution of PV$^+$ interneurons was not random (**Fig. 5c**; 93.3% of the comparisons between experimental and simulated data sets had a *P* < 0.01, Kolmogorov-Smirnov, *n* = 15). Identification of individual clusters in each brain using

agglomerative hierarchical clustering methods revealed that clusters of PV$^+$ interneurons had an organization very similar to that found in *Nkx2-1-Cre* mice (72.80 ± 2.04% of interneurons in clusters, *n* = 10; 70.50 ± 3.70 clusters per data set, *n* = 10). For example, the average distance between PV$^+$ interneurons in a cluster was also around 400 μm (**Fig. 5d**; mean threshold value 393 ± 11 μm, *n* = 14). In addition, most cell clusters contained interneurons confined to one or, at most, two adjacent layers of the cortex (intralaminar, 45.90 ± 2.71%; adjacent interlaminar, 45.07 ± 1.84%; **Fig. 5e**) and were typically located in deep layers of the neocortex (clusters in layer V or VI, 95.36 ± 1.05%; *n* = 10; **Fig. 5f**).
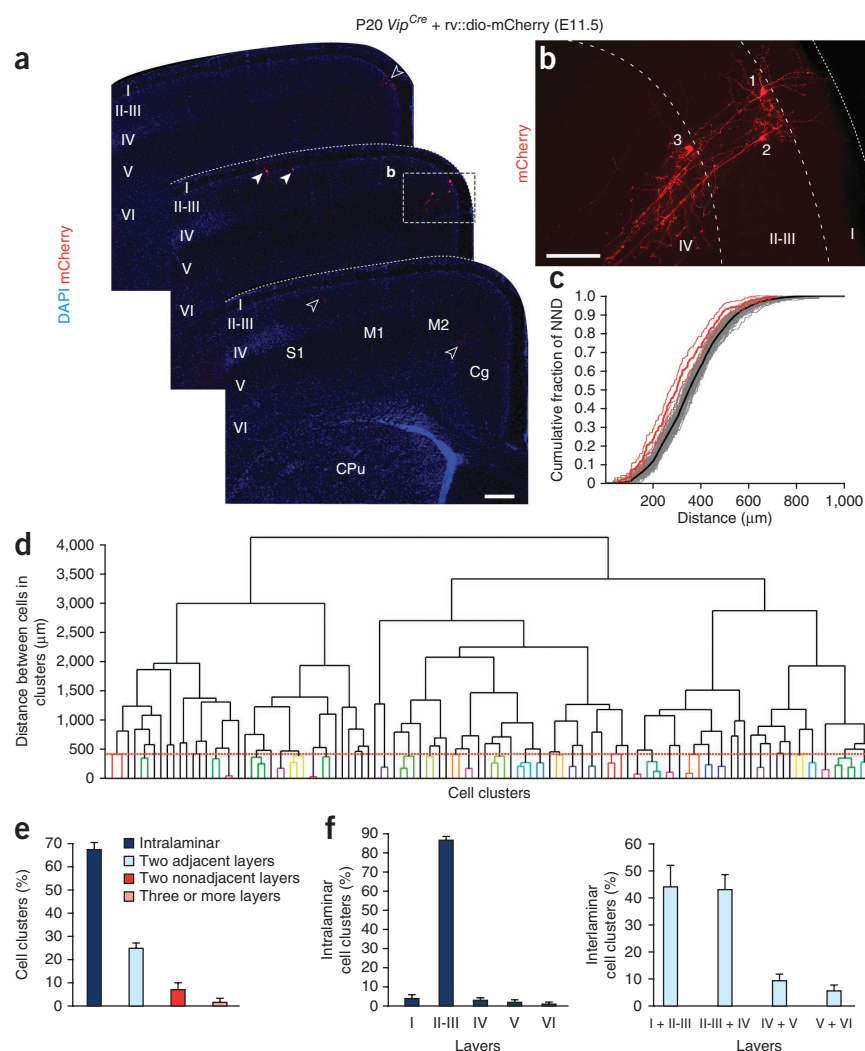
Analysis of the neocortex of P20 *Sst*^{Cre} mice infected with conditional retroviruses at E11.5 yielded very similar results. We found that many labeled SST$^+$ interneurons clustered throughout the neocortex (**Fig. 6a–c**). NND analyses confirmed that the distribution of clonally related SST$^+$ interneurons was not random (**Fig. 6d**; 87.5% of the comparisons between experimental and simulated data sets had a *P* < 0.01, Kolmogorov-Smirnov, *n* = 16). Clustering analysis revealed a large fraction of clustered interneurons (69.33 ± 2.81% of interneurons in clusters, *n* = 7; 70.29 ± 12.44 clusters per data set,

Figure 6 Clustering of SST$^+$ interneurons in the cerebral cortex. (**a–c**) Serial coronal sections (100 μm thick) through the telencephalon of a P20 *Sst*^{Cre} mouse infected with low-titer conditional reporter retroviruses at E11.5 and stained with DAPI and antibodies against mCherry. Two clusters are shown (**b** and **c**), containing two (labeled 1 and 2; **b**) and four (labeled 1 to 4; **c**) interneurons, respectively. Dashed lines define external brain boundaries in **a** and cortical layers in **b,c**. (**d**) Cumulative NNDs for an example population taken from one *Sst*^{Cre} mouse, with experimental (heavy red line) and simulated (black line) distributions. Light red lines delineate a *P* = 0.05 confidence interval for the experimental distribution; gray lines depict 100 random repetitions for the simulated distribution. Kolmogorov-Smirnov two-sample test, *P* = 3.04 × 10^{-10}. (**e**) Dendrogram showing the hierarchical relationship between labeled SST$^+$ interneurons grouped according to their distances using agglomerative hierarchical clustering. The purple dotted line indicates the threshold value that defines clustering for this experiment. (**f**) Quantification of the relative abundance of intralaminar and interlaminar (two adjacent, two nonadjacent, and three or more layers) interneuron clusters. (**g**) Quantification of the laminar distribution of intralaminar and interlaminar (two adjacent layers only) interneuron clusters. I–VI, cortical layers I to VI; CPu, caudoputamen nucleus; S1, primary somatosensory cortex; S2, secondary somatosensory cortex. Scale bars, 300 μm (**a**), 100 μm (**b,c**; same magnification). Histograms depict mean ± s.e.m.
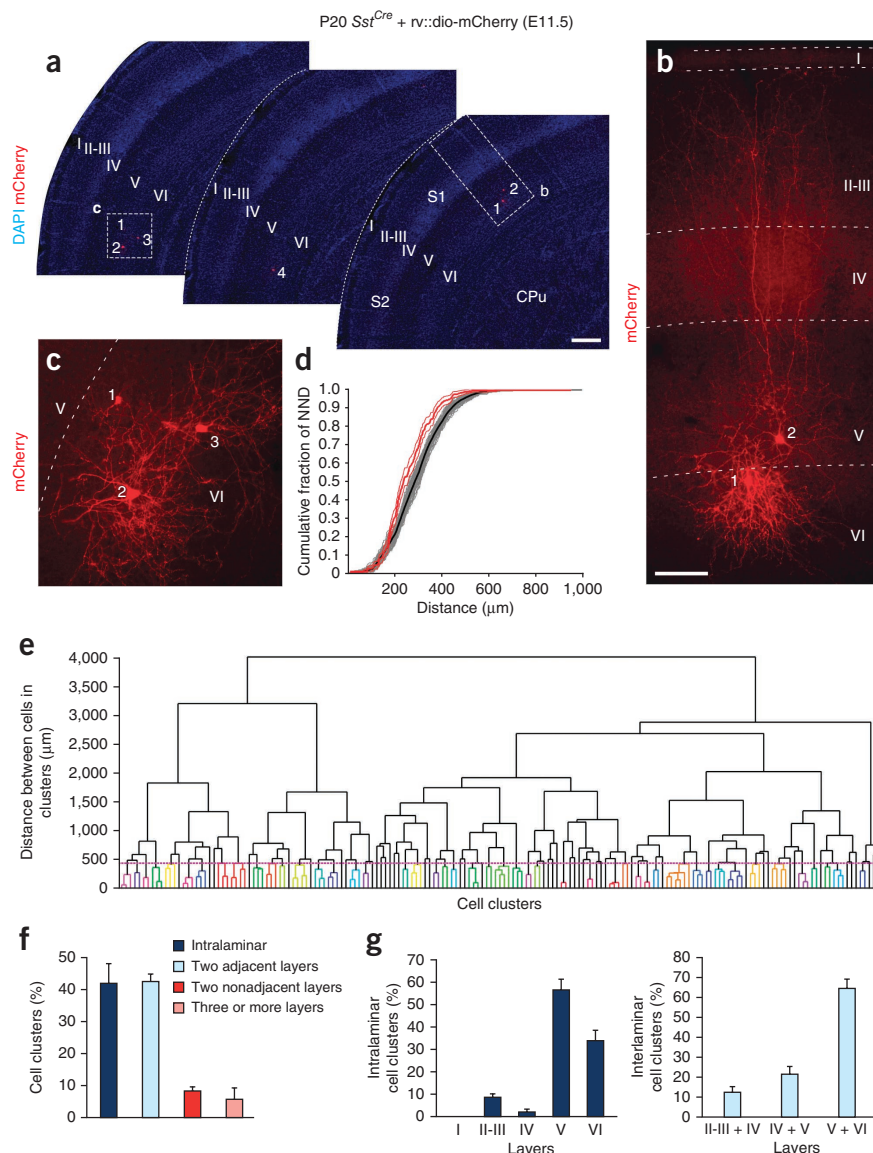
Figure 7 Clustering of VIP+ interneurons in the cerebral cortex. (**a,b**) Serial coronal sections (100 μm thick) through the telencephalon of a P20 *Vip*^Cre mouse infected with low-titer conditional reporter retroviruses at E11.5 and stained with DAPI and antibodies against mCherry. Three labeled interneurons (labeled 1 to 3) form a cluster confined to a single section. These neurons are shown at high magnification in **b**. Solid arrowheads in **a** point to other labeled interneurons; open arrowheads indicate the dendrites of interneurons labeled in other sections. Dashed lines define external brain boundaries in **a** and cortical layers in **b**. (**c**) Cumulative NNDs for an example population taken from one *Vip*^Cre mouse, with experimental (heavy red line) and simulated (black line) distributions. Light red lines delineate a $P = 0.05$ confidence interval for the experimental distribution; gray lines depict 100 random repetitions for the simulated distribution. Kolmogorov-Smirnov two-sample test, $P = 3.22 \times 10^{-8}$. (**d**) Dendrogram showing the hierarchical relationship between labeled PV+ interneurons grouped according to their distances using agglomerative hierarchical clustering. The red dotted line indicates the threshold value that defines clustering for this experiment. (**e**) Quantification of the relative abundance of intralaminar and interlaminar (two adjacent, two nonadjacent, and three or more layers) interneuron clusters. (**f**) Quantification of the laminar distribution of intralaminar and interlaminar (two adjacent layers only) interneuron clusters. I–VI, cortical layers I to VI; Cg, cingulate cortex; CPu, caudoputamen nucleus; M1, primary motor cortex; M2, secondary motor cortex; S1, primary somatosensory cortex. Scale bars, 300 μm (**a**), 100 μm (**b**). Histograms depict mean ± s.e.m.

$n = 7$), with an average distance between SST+ interneurons in a cluster in the same range as that of PV+ interneurons (**Fig. 6e**; mean threshold value 395 ± 23 μm, $n = 13$). As in the case of PV+ interneuron clusters, most SST+ interneuron clusters were confined to one or, at most, two adjacent layers of the cortex (intralaminar, $42.59 \pm 5.77\%$; adjacent interlaminar, $43.26 \pm 2.24\%$, $n = 7$; **Fig. 6f**) and were preferentially distributed through the deep layers of the neocortex (clusters in layer V or VI, $90.77 \pm 1.73\%$; $n = 7$; **Fig. 6g**). Altogether, these experiments demonstrate that lineages of the two main classes of MGE/POA-derived cortical neurons, PV+ and SST+ interneurons, cluster in the cerebral cortex.

CGE-derived interneurons also cluster in the cortex

We wondered whether this phenomenon is exclusive to MGE/POA-derived cortical interneurons. To explore this idea, we carried out a new set of experiments in *Vip*^Cre mouse embryos at E11.5. VIP+ interneurons derive from the CGE[36], so the lineage analysis of these interneurons should address that question.

Analysis of the neocortex of P20 *Vip*^Cre mice infected with conditional retroviruses at E11.5 revealed that labeled VIP+ interneurons also had a tendency to cluster throughout the neocortex ($66.09 \pm 2.65\%$ of interneurons in clusters, $n = 9$; **Fig. 7a,b**). Accordingly, NND comparisons between experimental and simulated data sets confirmed that the distribution of VIP+ interneurons was not random

(**Fig. 7c**; 69% of the comparisons between experimental and simulated data sets had a $P < 0.01$, Kolmogorov-Smirnov, $n = 13$). The average number of clusters was relatively consistent with the other experiments (46.09 ± 10.25 clusters per data set, $n = 11$). Clustering analysis indicated that the average distance between VIP+ interneurons in a cluster was approximately 400 μm (**Fig. 7d**; mean threshold value 374 ± 25 μm, $n = 9$), in the same range as that of MGE/POA-derived interneurons. Furthermore, VIP+ interneurons in most clusters were confined to one or, less frequently, two adjacent layers of the cortex (intralaminar, $66.68 \pm 2.84\%$; adjacent interlaminar, $24.35 \pm 1.78\%$; $n = 11$; **Fig. 7e**). However, in contrast to MGE/POA-derived clusters, VIP+ interneurons accumulated preferentially in superficial layers of the neocortex (clusters in layer II-III, $88.92 \pm 1.99\%$; $n = 11$; **Fig. 7f**). These results revealed that interneuron clustering is common to distinct classes of cortical interneurons, independently of their developmental origin.

Late-born MGE/POA-derived interneurons cluster in upper layers

Finally, we tested whether interneuron clustering was a specific property of early lineages in the subpallium. To this end, we performed low-titer injections of conditional reporter retroviral stocks into the lateral ventricle of E14.5 *Nkx2-1-Cre* embryos and examined the distribution of labeled interneurons in the neocortex of P20 mice. We found that most labeled interneurons clustered throughout the

Figure 8 Late born MGE/POA-derived interneurons cluster in superficial cortical layers. (**a**–**c**) Serial coronal sections (100 µm thick) through the telencephalon of a P20 *Nkx2-1-Cre* mouse infected with low-titer conditional reporter retroviruses at E14.5 and stained with DAPI and antibodies against GFP. Four labeled interneurons (labeled 1 to 4) form a compact cluster that spans two adjacent sections. These neurons are shown at high magnification in **b**,**c**. Dashed lines define external brain boundaries in **a** and cortical layer in **b**. (**d**) Cumulative NNDs for an example population taken from one *Nkx2-1-Cre* mouse, with experimental (heavy red line) and simulated (black line) distributions. Light red lines delineate a $P = 0.05$ confidence interval for the experimental distribution; gray lines depict 100 random repetitions for the simulated distribution. Kolmogorov-Smirnov two-sample test, $P = 1.52 \times 10^{-16}$. (**e**) Dendrogram showing the hierarchical relationship between labeled interneurons grouped according to their distances using agglomerative hierarchical clustering. The red dotted line indicates the threshold value that defines clustering for this experiment. (**f**) Quantification of the relative abundance of intralaminar and interlaminar (two adjacent, two nonadjacent, and three or more layers) interneuron clusters. (**g**) Quantification of the laminar distribution of intralaminar and interlaminar (two adjacent layers only) interneuron clusters. I–VI, cortical layers I to VI; CA1, hippocampus CA1 area; CA3, hippocampus CA3 area; V1, primary visual cortex; V2, secondary visual cortex. Scale bars, 300 µm (**a**), 100 µm (**b**,**c**). Histograms depict mean ± s.e.m.

neocortex (**Fig. 8a**–**c**). NND analyses confirmed that the distribution of these interneurons was not random (**Fig. 8d**; 100% of the comparisons between experimental and simulated data sets had a $P < 0.01$, Kolmogorov-Smirnov, $n = 11$). Clustering analysis revealed a large fraction of clustered interneurons (76.49 ± 1.36% of interneurons in clusters, $n = 11$; 86.82 ± 6.62 clusters per data set, $n = 11$), with an average distance between late-born interneurons in a cluster within the same range as that of early-born interneurons (**Fig. 8e**; mean threshold value 386.36 ± 15 µm, $n = 11$). Late-born interneuron clusters were also primarily confined to one or, at most, two adjacent layers of the cortex (intralaminar, 55.77 ± 2.02%; adjacent interlaminar, 35.96 ± 1.81%, $n = 11$; **Fig. 8f**). However, in contrast to those in E11.5 infections, interneuron clusters were preferentially distributed through the superficial layers of the neocortex (clusters in layer II-III or IV: 94.58 ± 1.79%; $n = 11$; **Fig. 8g**). These experiments reinforced the view that at least two separated lineages of progenitor cells exist in MGE/POA, devoted respectively to the generation of interneurons for deep and superficial layers of the cortex.

DISCUSSION

Our results demonstrate that GABAergic interneurons do not distribute randomly throughout the cortex. Instead, interneurons have a tendency to form clusters that occupy a relatively small volume of cortical tissue, a behavior that seems universal across all three major classes of interneurons (PV+, SST+ and VIP+). Although the
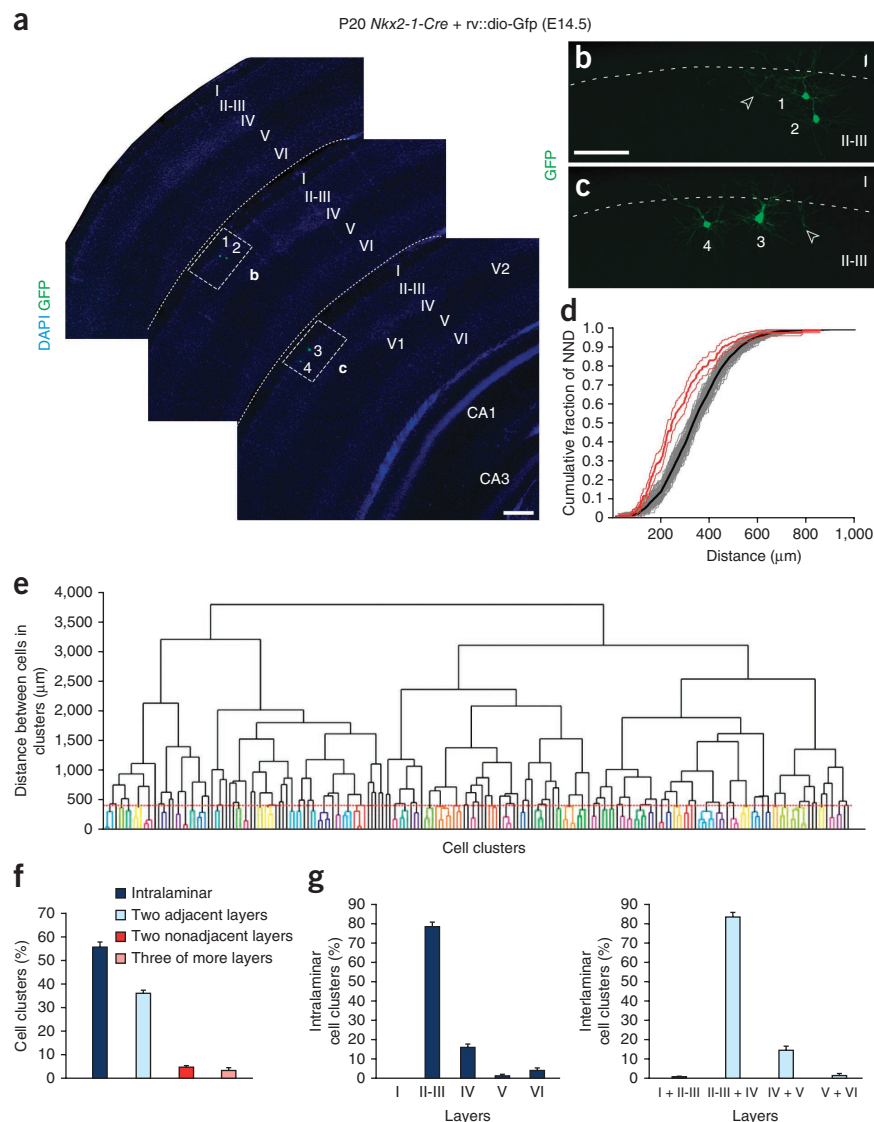
mechanisms underlying the clustering of interneurons in the cortex remain unclear, our experiments suggest that this process is not univocally linked to their shared clonal origin. Our analysis further indicate that different progenitor cells in the subpallium are committed to generate lineages of interneurons with restricted laminar distributions, which provides an unexpected view of cortical neurogenesis (**Supplementary Fig. 7**).

Methodological considerations

One caveat concerning retroviral tracing analyses is the lack of regional or cellular specificity. Here we have developed an approach to achieve clonal labeling with regional and cellular specificity that exclusively relies on Cre-expressing strains. To this end, we generated conditional retroviruses in which expression of a reporter protein requires Cre-mediated recombination. Our experiments demonstrate that this method can be used to perform lineage analyses for identified populations of progenitor cells or even entire cohorts of postmitotic neurons.

The retrovirus used in this study randomly integrates into one daughter cell after infection, which means that in roughly 50% of the cases infected clones will be incompletely labeled. We would predict

that this 'noise' labeling should interfere with the identification of interneuron clusters. Consistent with this idea, we observed in each experiment that a relatively large fraction (~30%) of interneurons did not seem to associate with any particular cluster. Despite this experimental limitation, our statistical analyses revealed highly significant differences with random distributions for all classes of cortical interneurons, which suggests that interneuron clustering is a very robust process.

Clustering is a property of different types of interneuron

Our experiments suggest that interneuron lineages have a strong tendency to reside roughly in the same location within the cerebral cortex. This finding independently replicates recent work on the organization of MGE/POA-derived interneurons in the neocortex[29] but, in addition, generalizes this concept to all main classes of cortical inhibitory cells. These results indicate that interneuron clustering is a universal phenomenon for cortical GABAergic interneurons, independently of their embryonic origin.

Clustering did not seem to be equally robust for the three main classes of interneurons (**Supplementary Fig. 8**). Clustering of PV[+] interneurons seemed stronger than for SST[+] and VIP[+] interneurons. While this may simply reflect intrinsic differences in the behavior of distinct interneuron lineages, alternative explanations may exist. For example, it is conceivable that both SST[+] and VIP^{+} cells are generated as part of larger, mixed clones containing other classes of interneurons. This seems to be the case for SST[+] interneurons, which are often found in mixed clones with PV[+] interneurons, and it could also be the case for VIP[+] interneurons, as other classes of interneurons are simultaneously generated in the CGE[11,17,36,37]. In contrast, many PV[+] interneurons seem to arise from homogeneous clones, which are therefore larger and easier to identify.

It has been previously suggested that interneuron clustering is directly related to lineage relationships[29]. However, our 'cocktail' experiments using GFP[+] and mCherry[+] retroviruses indicated that many interneuron clusters might contain cells derived from two adjacent progenitor cells. These results suggest that interneuron clustering might not be strictly determined by lineage relationships but rather by the non–cell-autonomous sharing of migratory cues. This hypothesis is supported by the observation that most cells in a cluster tended to be synchronously generated and might therefore migrate to the cortex using the same guidance mechanisms. Obviously, clonally related interneurons born roughly at the same time will also share the same environment and therefore will have a strong tendency to cluster, but lineage *per se* might not be the key factor controlling their clustering.

The mechanisms leading to the formation of interneuron clusters remains to be addressed experimentally, but on the basis of our observations it is tempting to speculate that interneurons born roughly at the same time from adjacent progenitor cells would end up in approximately the same region of the neocortex. This solution implies that there is some sort of topographical organization relating the subpallium and the neocortex, which is preserved during the tangential migration of interneurons to the cortex. Radial migration is an effective mechanism for preserving topographical relationships between the ventricle and the mantle[38], but it is unclear how tangential migration would guarantee this process.

Layer-specific interneuron lineages

One of the most intriguing findings of our lineage analysis is that interneurons labeled after E11.5 and E14.5 viral infections consistently clustered in the same or in two adjacent layers, either in infragranular layers (E11.5 MGE/POA-derived interneurons) or in superficial layers of the cortex (E14.5 MGE/POA-derived interneurons and CGE-derived interneurons). In other words, interneuron clusters did not typically extend through the entire thickness of the cerebral cortex. This is in sharp contrast with recent findings from the Shi laboratory[29], which concluded that the clonal production of interneurons is somehow linked to the vertical, columnar organization of the neocortex. We believe that the origin of this discrepancy is methodological and due to the use of different criteria for the classification of interneuron clusters. On the basis of the observation that most interneuron clusters cover a range of roughly 300 μm (a measurement that is within the range of our observations), Brown and colleagues[29] defined a cuboidal matrix to identify horizontal and vertical interneuron clusters, which measured 300 μm on the side of the tangential plane but used the entire thickness of the cortex in the radial dimension (~1 mm). This method is biased in favor of scoring groups of interneurons as vertical clusters because it brings together neurons that are more distant in the radial dimension (up to 1 mm) than in the tangential plane (300 μm). In contrast, we used an unbiased approach that is completely adimensional, as it relies only on the net distances between neurons to report clustering preferences. Using this method, we came to the conclusion that most interneurons group in one or two adjacent layers. This is not simply a semantic discrepancy. We recognized that many of the clusters we observed had a 'vertical' appearance even when including cells within the same layer. However, we believe that what is biologically relevant in this context is that clusters consistently mapped into infragranular or supragranular layers of the cortex but very rarely expanded across these layers.

The restricted laminar organization of interneuron clusters is not entirely surprising for VIP[+] interneurons because it is well established that most CGE-derived interneurons end up in superficial layers of the cortex[36]. However, MGE/POA-derived interneurons colonize the entire thickness of the cortex[13,14], and so it was unexpected to find that interneuron lineages labeled by E11.5 viral injections were largely confined to deep layers of the cortex. Notably, this observation is not influenced by our clustering analysis because laminar distributions are independent of whether labeled cells are classified as part of a cluster or not (**Supplementary Fig. 9**).

These results have important implications for the organization of cortical GABAergic interneurons (**Supplementary Fig. 7**). First, they imply that the progenitor cells that are present in the MGE/POA at E11.5 do not contribute much to the generation of interneurons for superficial layers of the cortex, which in turn suggests that different progenitor cells must exist to produce interneurons for deep and superficial cortical layers. This idea is further supported by the observation that layer I interneurons are exclusively generated from progenitor cells located in the POA and CGE but not in the MGE[13–15,36]. We favor the hypothesis that interneuron lineages devoted to deep and superficial layers of the cortex segregate before E11.5 and have different proliferation dynamics. Accordingly, both types of progenitors would coexist in the ventricular zone at E11.5, but in very different proportions. This possibility would imply that the distinct types of progenitor cells would lead to partly overlapping waves of neurogenesis for the generation of deep and superficial layer interneurons. This hypothesis is compatible with the observed shift in the production of particular interneuron subtypes in the MGE during development[39].

Excitatory and inhibitory neuronal assemblies in the cortex

Proper functioning of the neocortex depends critically on the balance between excitatory pyramidal cells and inhibitory GABAergic interneurons[40,41]. Considering the tremendous heterogeneity of both pyramidal cells and interneurons[42,43], precise mechanisms must exist

that enable the formation of excitatory and inhibitory cell assemblies in the cerebral cortex in a layer-to-layer and region-to-region basis.

Neocortical pyramidal cells are organized along two main axes, horizontal layers and vertical columns. Distinct classes of pyramidal cells occupy different layers, and layers are vertically linked into columns through coherent sets of functional connections[4,5]. These layer-specific classes of cortical excitatory neuron derive from radial glial progenitor cells in sequential order, with neurons destined for deep layers being generated first, followed by superficial layer neurons. It is commonly accepted that the fate of pyramidal cells is related to their birthdate, which progressively restricts the neurogenic potential of a common radial glial progenitor[8,38]. The radial unit hypothesis also establishes a basis for the generation of functional columns in the cortex because clonally related pyramidal cells seem to establish preferential connections and respond to common sensory stimuli[44–46]. However, this view has been recently challenged by the discovery of distinct lineages of ventricular zone progenitor cells that are intrinsically specified to generate pyramidal cells for different cortical layers[47,48]. In line with this notion, our study suggests that deep- and superficial-layer interneurons also derive from separate lineages of progenitor cell. Thus, a common theme is emerging on the organization of the cerebral cortex that links its laminar dimension to the fate specification of progenitor cells.

It has been thought that cortical GABAergic interneurons may somehow be organized in relation to pyramidal cells[20,34,49,50]. Our results support the idea that progenitor cells in the subpallium generate interneurons whose spatial organization reflects the laminar distribution of pyramidal cells. This observation is consistent with the idea that the laminar position of different cortical interneurons, at least those emerging from the MGE, is regulated by layer-specific or even cell type–specific cues produced by pyramidal cells[34,49,50]. Although our results support a general model for the matching of deep- and superficial-layer interneurons and pyramidal cells, the existence of distinct lineages of cortical interneurons in the developing subpallium might allow for an even more specific coordination in the assembly of excitatory and inhibitory neuronal populations in the cerebral cortex.

METHODS

Methods and any associated references are available in the online version of the paper.

Note: Any Supplementary Information and Source Data files are available in the online version of the paper.

AUTHORS CONTRIBUTIONS

G.C., M.M. and O.M. designed the project; G.C., N.D. and I.S. performed the research and analyzed the results; Z.J.H., M.M. and O.M. provided analytical tools, reagents and transgenic mice. G.C., M.M. and O.M. interpreted the data and wrote the paper.

COMPETING FINANCIAL INTERESTS

The authors declare no competing financial interests.

Reprints and permissions information is available online at http://www.nature.com/reprints/index.html.

1. Klausberger, T. & Somogyi, P. Neuronal diversity and temporal dynamics: the unity of hippocampal circuit operations. *Science* **321**, 53–57 (2008).
2. Isaacson, J.S. & Scanziani, M. How inhibition shapes cortical activity. *Neuron* **72**, 231–243 (2011).
3. DeFelipe, J. & Fariñas, I. The pyramidal neuron of the cerebral cortex: morphological and chemical characteristics of the synaptic inputs. *Prog. Neurobiol.* **39**, 563–607 (1992).
4. Mountcastle, V.B. The columnar organization of the neocortex. *Brain* **120**, 701–722 (1997).
5. Jones, E.G. & Rakic, P. Radial columns in cortical architecture: it is the composition that counts. *Cereb. Cortex* **20**, 2261–2264 (2010).
6. Silberberg, G., Gupta, A. & Markram, H. Stereotypy in neocortical microcircuits. *Trends Neurosci.* **25**, 227–230 (2002).
7. Rakic, P. Guidance of neurons migrating to the fetal monkey neocortex. *Brain Res.* **33**, 471–476 (1971).
8. Noctor, S.C., Flint, A.C., Weissman, T.A., Dammerman, R.S. & Kriegstein, A.R. Neurons derived from radial glial cells establish radial units in neocortex. *Nature* **409**, 714–720 (2001).
9. Anderson, S.A., Eisenstat, D.D., Shi, L. & Rubenstein, J.L.R. Interneuron migration from basal forebrain to neocortex: dependence on Dlx genes. *Science* **278**, 474–476 (1997).
10. Marín, O. & Rubenstein, J.L.R. A long, remarkable journey: tangential migration in the telencephalon. *Nat. Rev. Neurosci.* **2**, 780–790 (2001).
11. Butt, S.J. *et al.* The temporal and spatial origins of cortical interneurons predict their physiological subtype. *Neuron* **48**, 591–604 (2005).
12. Flames, N. *et al.* Delineation of multiple subpallial progenitor domains by the combinatorial expression of transcriptional codes. *J. Neurosci.* **27**, 9682–9695 (2007).
13. Fogarty, M. *et al.* Spatial genetic patterning of the embryonic neuroepithelium generates GABAergic interneuron diversity in the adult cortex. *J. Neurosci.* **27**, 10935–10946 (2007).
14. Xu, Q., Tam, M. & Anderson, S.A. Fate mapping Nkx2.1-lineage cells in the mouse telencephalon. *J. Comp. Neurol.* **506**, 16–29 (2008).
15. Gelman, D.M. *et al.* The embryonic preoptic area is a novel source of cortical GABAergic interneurons. *J. Neurosci.* **29**, 9380–9389 (2009).
16. Wichterle, H., Turnbull, D.H., Nery, S., Fishell, G. & Alvarez-Buylla, A. In utero fate mapping reveals distinct migratory pathways and fates of neurons born in the mammalian basal forebrain. *Development* **128**, 3759–3771 (2001).
17. Nery, S., Fishell, G. & Corbin, J.G. The caudal ganglionic eminence is a source of distinct cortical and subcortical cell populations. *Nat. Neurosci.* **5**, 1279–1287 (2002).
18. Yozu, M., Tabata, H. & Nakajima, K. The caudal migratory stream: a novel migratory stream of interneurons derived from the caudal ganglionic eminence in the developing mouse forebrain. *J. Neurosci.* **25**, 7268–7277 (2005).
19. Rymar, V.V. & Sadikot, A.F. Laminar fate of cortical GABAergic interneurons is dependent on both birthdate and phenotype. *J. Comp. Neurol.* **501**, 369–380 (2007).
20. Miyoshi, G. & Fishell, G. GABAergic interneuron lineages selectively sort into specific cortical layers during early postnatal development. *Cereb. Cortex* **21**, 845–852 (2011).
21. Wonders, C.P. & Anderson, S.A. The origin and specification of cortical interneurons. *Nat. Rev. Neurosci.* **7**, 687–696 (2006).
22. Hendry, S.H., Jones, E.G. & Emson, P.C. Morphology, distribution, and synaptic relations of somatostatin- and neuropeptide Y-immunoreactive neurons in rat and monkey neocortex. *J. Neurosci.* **4**, 2497–2517 (1984).
23. Cavanagh, M.E. & Parnavelas, J.G. Development of vasoactive-intestinal-polypeptide-immunoreactive neurons in the rat occipital cortex: a combined immunohistochemical-autoradiographic study. *J. Comp. Neurol.* **284**, 637–645 (1989).
24. Ma, Y., Hu, H., Berrebi, A.S., Mathers, P.H. & Agmon, A. Distinct subtypes of somatostatin-containing neocortical interneurons revealed in transgenic mice. *J. Neurosci.* **26**, 5069–5082 (2006).
25. Miller, M.W. Cogeneration of retrogradely labeled corticocortical projection and GABA-immunoreactive local circuit neurons in cerebral cortex. *Brain Res.* **355**, 187–192 (1985).
26. Fairén, A., Cobas, A. & Fonseca, M. Times of generation of glutamic acid decarboxylase immunoreactive neurons in mouse somatosensory cortex. *J. Comp. Neurol.* **251**, 67–83 (1986).
27. Ang, E.S. Jr., Haydar, T.F., Gluncic, V. & Rakic, P. Four-dimensional migratory coordinates of GABAergic interneurons in the developing mouse cortex. *J. Neurosci.* **23**, 5805–5815 (2003).
28. Tanaka, D.H. *et al.* Random walk behavior of migrating cortical interneurons in the marginal zone: time-lapse analysis in flat-mount cortex. *J. Neurosci.* **29**, 1300–1311 (2009).
29. Brown, K.N. *et al.* Clonal production and organization of inhibitory interneurons in the neocortex. *Science* **334**, 480–486 (2011).
30. Walsh, C. & Cepko, C.L. Clonally related cortical cells show several migration patterns. *Science* **241**, 1342–1345 (1988).

31. Sussel, L., Marín, O., Kimura, S. & Rubenstein, J.L. Loss of Nkx2.1 homeobox gene function results in a ventral to dorsal molecular respecification within the basal telencephalon: evidence for a transformation of the pallidum into the striatum. *Development* **126**, 3359–3370 (1999).

32. Cepko, C.L. *et al.* Lineage analysis using retroviral vectors. *Methods* **14**, 393–406 (1998).

33. Valcanis, H. & Tan, S.S. Layer specification of transplanted interneurons in developing mouse neocortex. *J. Neurosci.* **23**, 5113–5122 (2003).

34. Pla, R., Borrell, V., Flames, N. & Marín, O. Layer acquisition by cortical GABAergic interneurons is independent of Reelin signaling. *J. Neurosci.* **26**, 6924–6934 (2006).

35. Kawaguchi, Y. & Kubota, Y. GABAergic cell subtypes and their synaptic connections in rat frontal cortex. *Cereb. Cortex* **7**, 476–486 (1997).

36. Miyoshi, G. *et al.* Genetic fate mapping reveals that the caudal ganglionic eminence produces a large and diverse population of superficial cortical interneurons. *J. Neurosci.* **30**, 1582–1594 (2010).

37. Xu, Q., Cobos, I., De La Cruz, E., Rubenstein, J.L. & Anderson, S.A. Origins of cortical interneuron subtypes. *J. Neurosci.* **24**, 2612–2622 (2004).

38. Rakic, P. Specification of cerebral cortical areas. *Science* **241**, 170–176 (1988).

39. Miyoshi, G., Butt, S.J., Takebayashi, H. & Fishell, G. Physiologically distinct temporal cohorts of cortical interneurons arise from telencephalic Olig2-expressing precursors. *J. Neurosci.* **27**, 7786–7798 (2007).

40. Hensch, T.K. Critical period plasticity in local cortical circuits. *Nat. Rev. Neurosci.* **6**, 877–888 (2005).

41. Turrigiano, G. Too many cooks? Intrinsic and synaptic homeostatic mechanisms in cortical circuit refinement. *Annu. Rev. Neurosci.* **34**, 89–103 (2011).

42. Molyneaux, B.J., Arlotta, P., Menezes, J.R. & Macklis, J.D. Neuronal subtype specification in the cerebral cortex. *Nat. Rev. Neurosci.* **8**, 427–437 (2007).

43. Markram, H. *et al.* Interneurons of the neocortical inhibitory system. *Nat. Rev. Neurosci.* **5**, 793–807 (2004).

44. Yu, Y.C., Bultje, R.S., Wang, X. & Shi, S.H. Specific synapses develop preferentially among sister excitatory neurons in the neocortex. *Nature* **458**, 501–504 (2009).

45. Li, Y. *et al.* Clonally related visual cortical neurons show similar stimulus feature selectivity. *Nature* **486**, 118–121 (2012).

46. Ohtsuki, G. *et al.* Similarity of visual selectivity among clonally related neurons in visual cortex. *Neuron* **75**, 65–72 (2012).

47. Stancik, E.K., Navarro-Quiroga, I., Sellke, R. & Haydar, T.F. Heterogeneity in ventricular zone neural precursors contributes to neuronal fate diversity in the postnatal neocortex. *J. Neurosci.* **30**, 7028–7036 (2010).

48. Franco, S.J. *et al.* Fate-restricted neural progenitors in the mammalian cerebral cortex. *Science* **337**, 746–749 (2012).

49. Hevner, R.F., Daza, R.A., Englund, C., Kohtz, J. & Fink, A. Postnatal shifts of interneuron position in the neocortex of normal and reeler mice: evidence for inward radial migration. *Neuroscience* **124**, 605–618 (2004).

50. Lodato, S. *et al.* Excitatory projection neuron subtypes control the distribution of local inhibitory interneurons in the cerebral cortex. *Neuron* **69**, 763–779 (2011).

ONLINE METHODS

Mouse strains. *Nestin-Cre* (Jackson labs 003771), *Nkx2-1-Cre* (ref. 14), *Nkx2-1^CreERT2^*, *Sst^Cre^* and *Vip^Cre^* (ref. 51), *Pvalb^Cre^* (ref. 52), Rosa26 reporter CAG-boosted EGFP (*RCE*)[53] mice were kept at the Instituto de Neurociencias. All animal procedures were approved by the corresponding ethical committees (IN-CSIC and CEEA-PRBB) and were performed in accordance with Spanish (law 32/2007) and European regulations (EU directive 86/609, EU decree 2001-486). The day of vaginal plug was considered to be embryonic day (E) 0.5 and the day of birth postnatal day (P) 0.

DNA construct and retrovirus production. Cre-dependent conditional reporter retroviral constructs (rv::dio) were generated by subcloning a modified version of a double-floxed inverted open reading frame cassette[54] into BamH1 and PmeI restriction sites of a retroviral backbone kindly provided by F.H. Gage. This vector contains an internal CAG chicken β-actin promoter and the woodchuck hepatitis post-transcriptional regulatory element (WPRE), and encodes either GFP (enhanced) or membrane-bound (palmitoylation tag) mCherry as a reporter fluorescent protein. To visualize proliferating cells within interneuron clones, we used a fluorescent ubiquitylation-based cell cycle indicator system[55]. This Fucci indicator consists of a modified Azami Green fluorescent protein fused with a fragment of human geminin, which accumulates in the nucleus during S-G2-M phases but is rapidly degraded when cells progress to G1. In brief, we generated viruses encoding mCherry and a fragment of human geminin (1–110) fused with Azami Green (AM-V9014; MBL International Corporation) by using the P2A self-cleaving peptide as linker. Moloney murine leukemia viruses (MoMLV) were produced by transfecting HEK293T cells with the corresponding vectors along with CMV-vsvg and CMV-gagpol helper plasmids, and concentrated as previously described[56]. In the two-marker experiments (simultaneous injection of the GFP- and mCherry-encoding conditional reporter retroviruses), the two vectors were produced in the same plates and mixed before concentration by ultracentrifugation.

***In utero* retroviral infection.** Pregnant females were deeply anesthetized with isoflurane and E11.5 or E14.5 embryos, depending on the experiment, were individually injected using an ultrasound backscattering microscope (Visualsonic), as described previously[34]. Low-titer conditional retroviruses were released into the telencephalic ventricles using a nanoliter injector[57]. In birthdating experiments, pregnant females received intraperitoneal injections (three injections in 12 h) at E12.5 with 30 mg/kg EdU (5-ethynyl-2′-deoxyuridine, A10044 Invitrogen) and at E15.5 with 50 mg/kg BrdU (5-bromo-2′-deoxyuridine, B5002 Sigma-Aldrich). *Nkx2-1^CreERT2^;RCE* pregnant females received a single intraperitoneal injection of tamoxifen (2–3 mg/kg) diluted in corn oil at E11.5.

Immunohistochemistry. Postnatal mice were perfused transcardially with 4% paraformaldehyde (PFA) in PBS and the dissected brains were postfixed for 2 h at 4 °C in the same solution. Embryonic brains were dissected out in cold PBS and fixed in 4% PFA for 2–12 h. Postnatal brains were sectioned at 100 μm on a vibratome (VT1000S, Leica), while embryonic brains were sectioned at 50–60 μm. Free-floating coronal sections were then subsequently processed for immunohistochemistry as previously described[34]. The following primary antibodies were used: rabbit anti-GFP (1:1,000; A11122, Molecular Probes), chicken anti-GFP (1:1,000; GFP-1020, Aves Labs), rabbit anti-DsRed (1:500; 632496, Clontech), rat anti-SST (1:200; MAB354, Millipore), mouse anti-PV (1:750; PARV-19, Sigma-Aldrich), rabbit anti-PV (1:4,000; PV-28, Swant), rabbit anti-GABA (1:1,000; A2052, Sigma-Aldrich), mouse anti-BrdU conjugated with Alexa Fluor 647 (1:1,000; B35133, Invitrogen), rabbit anti-Nkx2-1 (1:1,000; PA 0100, Biopat), and rabbit anti-Ki67 (1:200; NCL-Ki67p, Novocastra). Cell nuclei were stained with 5 μM 4′-6-diamidino-2-phenylindole (DAPI) in PBS and sections mounted with Mowiol (Sigma) with NPG (Calbiochem). For mCherry/EdU/BrdU triple stainings, sections were first processed for mCherry immunohistochemistry, then fixed 20 min with 4% PFA in PBS and subsequently processed for EdU and BrdU staining. Tissue treatment for BrdU staining was performed as previously described[34]. EdU+ cells were detected using the Click-iT EdU Imaging kit (Molecular Probes) with Alexa Fluor 488. For immunohistochemistry after electrophysiological recordings, slices were fixed immediately after recording in 4% PFA at 4 °C from 2–12 h. Biocytin was revealed using ABC complex (1:100; Abcys). mAG-hGem protein expression was visualized without antibody staining.

Serial section reconstruction. To obtain a three-dimensional reconstruction of the telencephalon, each slice was plotted in serial order from rostral to caudal using a fluorescence microscope coupled to a Neurolucida system (MBF Bioscience). The external boundaries of each slice, as well as the neocortex, hippocampus and striatum, were traced. Each interneuron was identified with a unique code that reflected its precise position. Serial reconstructions were then obtained by aligning each section of the brain with the previous traces. The Cartesian coordinates (x, y, z) of each cell and the cell contour were then extracted and used for the analyses of cell distributions and clustering.

Electrophysiological recordings. P20–P30 *Nkx2-1-Cre* mice that were injected at E11.5 with rv:dio-Gfp were deeply anesthetized with isoflurane, decapitated and the brain rapidly removed and placed in ice-cold oxygenated solution consisting of (in mM) 248 sucrose, 3 KCl, 0.5 CaCl$_2$, 4 MgCl$_2$, 1.25 NaH$_2$PO$_4$, 26 NaHCO$_3$ and 10 glucose, saturated with 95% O$_2$ and 5% CO$_2$. Coronal slices (300 μm) were cut through the somatosensory cortex using a vibratome (Leica). The slices were then maintained at room temperature in artificial cerebrospinal fluid (ACSF) consisting of (in mM) 124 NaCl, 3 KCl, 2 CaCl$_2$, 1 MgCl$_2$, 1.25 NaH$_2$PO$_4$, 26 NaHCO$_3$ and 10 glucose, saturated with 95% O$_2$ and 5% CO$_2$. For patch-clamp recordings in whole-cell configuration, slices were transferred to a chamber and continuously superfused with ACSF at 32 °C. Cells were visualized with infrared-differential interference optics (Hamamatsu camera controller) viewed through a 40× water-immersion objective (Olympus). Patch microelectrodes (6–10 MΩ) were pulled from borosilicate glass (1.5 mm outer diameter, 0.86 mm inner diameter; Harvard Apparatus) using a vertical P10 puller (Narishige) and filled with a potassium gluconate–based intracellular solution containing (in mM) 140 potassium gluconate, 10 HEPES, 2 NaCl, 4 KCl, 4 ATP, 0.4 GTP and 0.6 Alexa 555. Biocytin (2–5 mg/ml) was added for post-recording immunocytochemistry. For targeting, GFP+ cells were excited at 488 nm. Interneurons were kept under current-clamp configuration with an Axoclamp 200A amplifier operating in a fast mode. Data were filtered online at 2 kHz and were acquired at a 20 kHz sampling rate using pClamp 6.0.2 software (Molecular Devices). Resting membrane potential, membrane resistance and membrane conductance were rapidly measured after patching the GFP+ interneurons. We analyzed offline in Clampfit 10.2 the action potential traces and calculated the following parameters: spike threshold potential, action potential amplitude, duration of the action potential at its half amplitude, AHP amplitude, maximum firing frequency (average frequency elicited by the maximum 500 ms current injection), onset frequency (first or second inter-spike interval), steady-state frequency (average of the last five inter-spike intervals), percentage of spike frequency adaptation (percentage of reduction between the first inter-spike frequency and the steady-state frequency). Data from cells with no action potentials were discarded. For the interneuron classification, we used the nomenclature proposed by the Petilla group[58]. We considered as "adapting" (AD) a cell with a percentage of spike frequency adaptation greater than 25%.

Imaging. Images were acquired using fluorescence microscopes (DM5000B/ CTR5000 and DMIRB; Leica) coupled to digital cameras (DC500 or DFC350FX, Leica; OrcaR2, Hamamatsu) or a confocal microscope (DMIRE2/ CTRMIC/TCS SP2; Leica). Neurolucida software (MBF Bioscience) was used for serial section reconstructions using a fluorescence microscope coupled to a digital camera (QICAM Fast 1394; QImaging).

Quantification of cell position and age. For the spatial distribution of interneuron clusters, the laminar position of each cell in the neocortex (identified by Cartesian coordinates) was recorded. Clusters of interneurons were classified according to the following categories: intralaminar cluster when all cells in the cluster were located in the same layer, and interlaminar cluster when cells in the cluster were localized in different layers. Interlaminar clusters were further subdivided into three groups: clusters spanning two adjacent layers, two nonadjacent layers, or three or more layers. In birthdating experiments, clusters were defined as isochronic when most cells in the cluster (>50%) were labeled with one of the markers (EdU or BrdU) and no cells were labeled with the other marker, or heterochronic when the cluster contained cells labeled with the two markers (EdU and BrdU). In the electrophysiological experiments, homogeneous and heterogeneous clusters were defined on the basis of intrinsic physiological properties

(FS and AD). Predominant and balanced cell clusters were defined on the basis of their relative composition of PV- and SST-expressing interneurons.

Statistical analysis of cell distributions and clustering. We first analyzed the distribution of interneurons in the neocortex by calculating nearest neighbor distances (NNDs). After determining the distance between each interneuron and the closest one, we compared these distances to the values expected for a sample of neurons located at random in the same volume (that is, the same neocortical hemisphere). Specifically, for each experiment, the experimental interneuron distribution was compared with 100 simulated distributions, generated by positioning the same number of elements at random locations distributed uniformly in the exact same region of tissue as the experimental condition. NNDs were displayed as cumulative distributions.

Interneuron clusters were defined and identified by applying an unsupervised agglomerative hierarchical clustering analysis[59], whereby interneurons were grouped according to their proximity. Results were displayed as hierarchical cluster trees or dendrograms. Specifically, dendrograms were built to visualize the hierarchical relationship of neurons according to their spatial distance. Starting from the initial condition in which each interneuron was an individual object, the closest objects were successively merged into clusters until only one cluster remained (the entire set of neurons). In the dendrogram, each node represented a merging point of cells into clusters or clusters into higher-level clusters. Two objects (cells or clusters) were merged into a single one depending on the average spatial distance between all their constituent neurons. The clustering analysis performed was exclusive (meaning that each cell was assigned to a single cluster). To identify experimental clusters, the results of the analysis for interneurons were compared to the same analysis applied to the 100 random simulated data sets. Clusters were accepted if the average distance between their constituent neurons (determined as above) fell below a threshold, determined as the distance that maximized the difference between the number of clusters in the experimental data set and the average number of clusters in the 100 simulated repetitions.

In our analyses, the sample size for each data set (hemisphere) represents the entire population of labeled interneurons in that experiment, with no exclusions. No statistical methods were used to predetermine sample size per experiment.

When the difference between NND distributions for experimental and simulated data sets was not significant, the result was scored as such; **Supplementary Figure 8** reports the dependence of test statistical significance on sample size. Biological replicates (*n* values are different populations derived from different brains from different litters) were analyzed to assess biological variability and reproducibility of data. The population size for biological replicates was similar to that generally employed in the field. NND cumulative distributions for experimental and simulated data sets were compared using the Kolmogorov-Smirnov two-sample test. This non-parametric test depends on differences in the shape of the empirical cumulative distribution. Testing was two-sided (the null hypothesis was no difference between the distributions), and statistical significance was set at $P < 0.01$. Results of clustering analyses were displayed as dendrograms and quantitative measurements were displayed as mean ± s.e.m.

NND and clustering analyses were performed using Matlab software (MathWorks).

51. Taniguchi, H. *et al.* A resource of Cre driver lines for genetic targeting of GABAergic neurons in cerebral cortex. *Neuron* **71**, 995–1013 (2011).
52. Hippenmeyer, S. *et al.* A developmental switch in the response of DRG neurons to ETS transcription factor signaling. *PLoS Biol.* **3**, e159 (2005).
53. Sousa, V.H., Miyoshi, G., Hjerling-Leffler, J., Karayannis, T. & Fishell, G. Characterization of Nkx6–2-derived neocortical interneuron lineages. *Cereb. Cortex* **19** (suppl. 1), i1–i10 (2009).
54. Cardin, J.A. *et al.* Driving fast-spiking cells induces gamma rhythm and controls sensory responses. *Nature* **459**, 663–667 (2009).
55. Sakaue-Sawano, A. *et al.* Visualizing spatiotemporal dynamics of multicellular cell-cycle progression. *Cell* **132**, 487–498 (2008).
56. Tashiro, A., Sandler, V.M., Toni, N., Zhao, C. & Gage, F.H. NMDA-receptor-mediated, cell-specific integration of new neurons in adult dentate gyrus. *Nature* **442**, 929–933 (2006).
57. Gaiano, N., Kohtz, J.D., Turnbull, D.H. & Fishell, G. A method for rapid gain-of-function studies in the mouse embryonic nervous system. *Nat. Neurosci.* **2**, 812–819 (1999).
58. Ascoli, G.A. *et al.* Petilla terminology: nomenclature of features of GABAergic interneurons of the cerebral cortex. *Nat. Rev. Neurosci.* **9**, 557–568 (2008).
59. Carugo, O. Clustering criteria and algorithms. *Methods Mol. Biol.* **609**, 175–196 (2010).